



Quest for Sunyaev-Zel'Dovich effect from the cosmic web at high resolution with MISTRAL

G. Isopi^{1,2}, E. Barbavara¹, E. S. Battistelli^{1,2}, P. de Bernardis^{1,2}, F. Cacciotti^{1,2}, V. Capalbo^{1,2}, A. Carbone¹, E. Carretti³, D. Ciccalotti¹, F. Columbro^{1,2}, A. Coppolecchia^{1,2}, A. Cruciani^{1,2}, G. D'Alessandro^{1,2}, M. De Petris^{1,2}, F. Govoni⁴, L. Lamagna^{1,2}, P. Marongiu⁴, A. Mascia⁴, S. Masi^{1,2}, E. Molinari⁵, M. Murgia⁴, A. Navarrini⁴, A. Novelli^{1,2}, A. Occhiuzzi¹, A. Orlati³, A. Paiella^{1,2}, G. Pettinari⁶, F. Piacentini^{1,2}, T. Pisanu⁴, S. Poppi⁴, I. Porceddu⁴, A. Ritacco^{4,7}, M. R. Schirru⁴, and G. Vargiu⁴

¹ Sapienza University of Rome, Italy

² Istituto Nazionale di Fisica Nucleare – Sezione di Roma I, Italy

³ Istituto Nazionale di Astrofisica – Istituto di Radioastronomia, Italy

⁴ Istituto Nazionale di Astrofisica – Osservatorio Astronomico di Cagliari, Italy

⁵ Istituto Nazionale di Astrofisica – Osservatorio Astronomico di Brera & REM, Italy

e-mail: giovanni.isopi@roma1.infn.it

The remaining affiliations can be found at the end of the paper.

Received: 2 December 2023; Accepted: 26 January 2024

Abstract. Baryonic matter, according to observations, accounts for 5% of our Universe. Half of this is undetected, and this discrepancy is known as “missing baryons problem”. Simulations predict that baryons could reside in the form of warm-hot intergalactic medium that constitutes a component of cosmic filaments, in a low-density, low-temperature state, thus difficult to observe. A tool to detect these baryons is the Sunyaev-Zel'Dovich effect arising from the interaction between cluster outskirts and the cosmic microwave background. Merging clusters are particularly interesting because their filaments are compressed, increasing their signal-to-noise ratio. Recent ground-based experiments allowed the study of filaments to arcminute scales. However, interesting science resides at small scales (10-20”), explorable with high resolution millimeter cameras. Here we present the status of the field and discuss future observations with the new MISTRAL camera, that will be an excellent instrument for the study of cosmic filaments.

Key words. Clusters, Cosmic Web, Sunyaev-Zel'Dovich effect

1. Introduction

The current paradigm in cosmology is the Λ CDM model, which has been extremely successful to date, being able to explain a wide range of phenomena with only 6 free parameters. Measurements of the cosmic microwave background (CMB) provided excellent estimates of these parameters (Aghanim et al. 2020), giving an insight on the fundamental composition of the universe. From these measurements we know that most of our universe is composed of dark energy and dark matter, while ordinary matter, or baryons, represent a mere 5% of the total mass-energy density. The baryon fraction is well constrained from these high-redshift measurements. However, when adding up all the baryons detectable in the late universe, a discrepancy is observed, as almost half of the baryons are undetected (Fukugita et al. 1998). The leading explanation for this discrepancy, supported by simulations, is that a significant part of the baryons reside outside galaxy clusters, in the filaments that form the “cosmic web” (Cen & Ostriker 2006). The cosmic web is a low-density, low-temperature environment, thus baryons are in a state known as warm-hot intergalactic medium (WHIM). Due to its physical characteristics, WHIM is difficult to detect. Indeed, the low temperature ($10^5 - 10^7$ K) and density ($\delta = 5 - 500^1$) greatly suppress the X-ray bremsstrahlung emission, while the faint magnetic field does not produce significant synchrotron emission. X-ray absorption studies, using cosmic beacons such as blazars, quasars or gamma-ray bursts afterglows (Tejos 2016), also allows the characterization of missing baryons. However, this method can not be used for large scale mapping. A complementary probe is the thermal Sunyaev-Zel’Dovich effect (Sunyaev & Zeldovich 1980) (tSZ), an anisotropic spectral distortion of the CMB produced by the scattering between low energy photons and high energy electron populations, like in the intra-cluster medium (ICM) or in cosmic filaments. The spectral distortion has a peculiar spectral

shape and has the unique characteristic of producing a negative temperature signal at frequencies below 217 GHz:

$$\frac{\Delta I(x)}{I_0} = y \frac{x^4 e^x}{(e^x - 1)^2} \left(x \coth \frac{x}{2} - 4 \right) := yg(x) \quad (1)$$

where $x = h\nu / (k_B T_{CMB})$, ν is the frequency, h is the Planck constant, k_B is the Boltzmann constant, T_{CMB} is the temperature of the CMB, and y is the comptonization parameter, which is proportional to the product between electron density n_e and electron temperature T_e integrated along the line-of-sight (LOS) (Mroczkowski et al. 2019):

$$y = \frac{\sigma_T}{m_e c^2} \int_{LOS} n_e(r) k_B T_e(r) dr \quad (2)$$

where σ_T is the Thomson scattering cross-section, m_e is the electron mass and c is the speed of light.

2. Filaments between clusters

An interesting environment in which it is possible to characterize WHIM is in the outskirts of pre-merger clusters. In this situation, a primordial filament can be compressed by the merging clusters, increasing their pressure thus their tSZ signal and X signal, allowing the structure to be directly observed. From now on we will refer to filaments between interacting clusters as “bridges”. The first detections of individual bridges using the tSZ effect were reported by the Planck satellite at a resolution of $10'$ (Ade et al. 2013). These detections included some known pairs of interacting clusters, most notably A401-A399 and A3391-A3395. In the first pair, a joint analysis with X-ray data provided an estimate of the electron temperature and density, which was found to be consistent with simulations. The same region was also studied in the radio domain, showing the presence of a radio “ridge” between the clusters (Govoni et al. 2009; Murgia et al. 2010). Although A399-A401 is a rather unique system, it represents a great laboratory to characterize the WHIM using a multi-instrument, multi-wavelength approach, given the large amount of independent observations.

¹ $\delta = \frac{(\rho - \bar{\rho})}{\bar{\rho}}$ is the matter overdensity, where ρ is the density of an overdense region and $\bar{\rho}$ is the average density of the universe at its redshift.

Another approach that was successfully applied to Planck data is stacking a large number of candidate interacting systems in order to increase the SNR and detect an average excess signal between clusters (de Graaff et al. 2019; Tanimura et al. 2019; Singari et al. 2020). Another example is the other notable detection by Planck, the A3391-A3395 system, that was observed in great detail by the eROSITA X-ray telescope with unprecedented depth and sensitivity (Reiprich et al. 2021). This observation allowed the distinction between hot ICM and warm, primordial gas. Due to the complexity of the system, the 10' resolution provided by Planck is rather inadequate, as the clusters are separated by 37', corresponding to few beams, and it does not allow a full, spatially resolved characterization.

3. High resolution tSZ observations

Observations provided by Planck gave the first tentative detections of warm-hot gas residing outside galaxy clusters. For a better characterization, higher resolution observations are required. An interesting example is still the A399-A401 cluster system, that was observed at arcminute resolution (1.65') by the Atacama Cosmology Telescope (ACT), providing the deepest tSZ observation of the system to date. The higher resolution allowed a better untangling of the bridge signal from cluster pressure profiles, that was detected with a significance better than 5σ . Additionally, this observation provided a better understanding of the 3D orientation of the system, which is not trivial to derive in most cases Hincks et al. (2021). Many other cluster pair candidates reside at higher redshift with separation of few arcminutes, thus being barely resolved by ACT Hilton et al. (2021). For this reason it is useful to observe them at higher resolution (10'') using millimeter cameras on large, single dish radio telescopes.

3.1. State of the art

Few instruments with such capabilities exist in the world. In the W band (75-110 GHz), the state of the art is the MUSTANG-2 cam-

era (Dicker et al. 2014) at the 100 m Green Bank Telescope (GBT), providing a 4.2' field of view (FOV) and a resolution of 9.5'' (Orlowski-Scherer et al. 2022). Another camera working in the W-band is the 100 GHz MKID Camera (Honda et al. 2023) at the 45 m Nobeyama Telescope, with a FOV of 3'. The latest deployed instrument of this kind is the MISTRAL camera at the 64 m Sardinia Radio Telescope (SRT), see section 4. Other notable instruments, working at higher frequencies, are TolTEC (Wilson et al. 2020) at the 50 m Large Millimeter Telescope, NIKA2 at the 30 m IRAM telescope (Perotto et al. 2020). See Table 1 for further details. Although interferometers provide higher resolution, their field of view is small ($< 1'$), and makes large maps unfeasible because of the long observation time needed. For this reason, single dish cameras are highly complementary to interferometers in tSZ observations (Mroczkowski et al. 2019).

3.2. Cluster and filaments at sub-arcmin resolution

Observations of clusters and filaments at high resolution can provide a deep understanding of the dynamics and thermodynamics of the ICM. In Hincks et al. (2021), observations at a resolution of 12.7'' with MUSTANG-2 gave an estimate of the amplitude of the pressure fluctuations in the A401 cluster and in the bridge region. The low amplitude of these fluctuations is compatible with a relaxed cluster, supporting the pre-merger scenario and a primordial origin of the filament between them. Untangling the dynamical state of the cluster and determining if it is relaxed or non relaxed is a very complex task, and high resolution observations are needed to break this degeneracy. The observation of sub-structures in clusters and filaments like shocks and cold fronts is also interesting for the understanding of the dynamics of a cluster and its outskirts. A notable example of a shock observed with the tSZ effect is the candidate merger shock in the El Gordo galaxy cluster, at a redshift of ≈ 0.9 , that was observed at a resolution of 3-6'' by the ALMA interferometer (Basu et al. 2016). Similar struc-

Table 1. State of the art instruments for high resolution tSZ observations.

Instrument	Frequency [GHz]	resolution ["]	FOV [']
MUSTANG-2	90	9	4.2
MISTRAL	90	12.2	4
NIKA2	150/260	18/11	6.5
ToI TEC	150/220/270	9.5/6.3/5	4
Nobeyama 100 GHz	100	16.7	3

tures in clusters at lower redshift are accessible by the single dish cameras mentioned before (Mroczkowski et al. 2019). Another interesting example is the candidate shock in the A399-A401 system that was tentatively detected in X-rays by the Suzaku satellite (Akamatsu et al. 2017). This shock is located in the bridge region and runs parallel to it. It was not detected by ACT because of the insufficient resolution, but an observation with MUSTANG-2 or MISTRAL could provide useful and complementary information to strengthen its detection and its nature. In this case, an high resolution camera could play the same role that ACT had played for Planck.

4. High resolution tSZ with MISTRAL

The Millimeter Sardinia radio Telescope Receiver based on Array of Lumped elements KIDs (MISTRAL) is a new W-band camera, that was installed in May 2023 at the gregorian focus of the SRT, and is currently undergoing the technical commissioning (Battistelli et al. 2023b,a). The receiver observes at ≈ 90 GHz with an array of 415 Kinetic Inductance Detectors (KIDs) in lumped configuration (LEKIDs) that fill a diffraction limited focal plane of ≈ 90 mm in diameter, corresponding to $\approx 4'$ in the sky (Paiella et al. 2022, 2023; Cacciotti et al. 2023). The detectors are cooled down to 200–240 mK by a four stage cryostat (Coppolecchia et al. 2023), custom built with strict requirements on weight and size (Fig. 1). The MISTRAL camera at the focus of the SRT provides a resolution of

$\approx 12''$. During the laboratory characterization phase, we used noise time-streams acquired with a background of 300 K as a worst-case scenario for the background that will hit the KIDs at the radio telescope, and we used it to estimate the noise equivalent flux density, equal to $2.8 \text{ mJy } \sqrt{s}$. This estimate assumes a complete removal of the correlated noise due to the atmosphere. The efficiency of the atmospheric removal depends on the scanning strategy, as well as the filtering and map-making pipeline, and will be further characterized during the commissioning phase. As a preliminary estimate, by re-scaling data obtained at SRT at 22 GHz, we found a range of values between 5–15 $\text{mJy } \sqrt{s}$. This reflects into a mapping speed of 170 – 1500 $\text{arcmin}^2/\text{mJy}^2/\text{h}$ (Isopi et al. 2023; Perotto et al. 2020).

5. Conclusions

High resolution observations at $\approx 10''$ represent a step forward in the understanding of the dynamics and thermodynamics of clusters and cosmic filaments, because of the high spatial resolution (tens of kpc) achievable. MISTRAL, a new receiver installed in May 2023 at the gregorian focus of SRT, will provide this resolution. It observes the W-band sky at a resolution of $12''$ using an array of 415 Kinetic Inductance Detectors, sampling a diffraction limited focal plane that spans $4'$ in the sky. The mapping speed presented in section 4 is comparable to other state of the art instruments: NIKA2 reports a mapping speed of 1400/110 $\text{arcmin}^2/\text{mJy}^2/\text{h}$ at 150/260 GHz

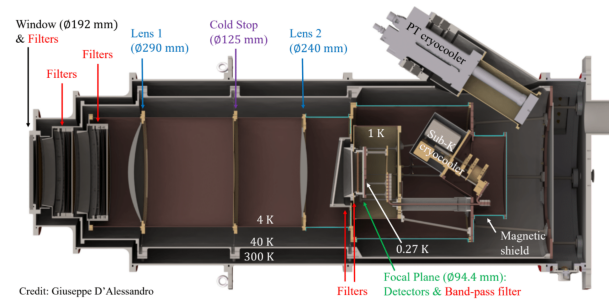


Fig. 1. CAD drawing of MISTRAL, showing its main subsystems (D'Alessandro et al. 2022).

(Perotto et al. 2020), MUSTANG-2 reports $\approx 500 \text{ arcmin}^2/\text{mJy}^2/\text{h}$ at 90 GHz (Romero 2021). This mapping speed allows MISTRAL to observe wide areas of the sky in few hours of observations, down to a sensitivity of $\approx \text{mJy}$. This sensitivity can also be translated into a Compton- γ sensitivity, by integrating the tSZ spectral distortion over the MISTRAL band. This can also be expressed in terms of Compton- γ sensitivity $\Delta\gamma \approx 2 \times 10^{-5}$ in 1 h of integration time (Isopi et al. 2023). Very few instruments of this kind exist in the world, and only two other instruments operate in the same frequency band at similar resolution. For this reason, MISTRAL will provide a precious new stream of data to the tSZ science community.

Affiliations

⁶ Istituto di Fotonica e Nanotecnologie (CNR), Italy

⁷ Laboratoire de Physique de l'École Normale Supérieure, Université PSL, CNRS, Sorbonne Université, Université de Paris, France

References

- Ade, P. A. R. et al. 2013, *A&A*, 550, A134
 Aghanim, N. et al. 2020, *A&A*, 641, A6
 Akamatsu, H. et al. 2017, in *The X-ray Universe 2017*, ed. J.-U. Ness & S. Migliari, 30
 Basu, K. et al. 2016, *ApJ*, 829, L23
 Battistelli, E. S. et al. 2023a, in *MG16*, 1542–1556
 Battistelli, E. S. et al. 2023b, arXiv e-prints, arXiv:2310.18029
 Cacciotti, F. et al. 2023, *JLTD*, in prep
 Cen, R. & Ostriker, J. P. 2006, *ApJ*, 650, 560
 Coppolecchia, A. et al. 2023, *JLTD*, in prep
 D'Alessandro, G. et al. 2022, in *EPJWP*, Vol. 257, *mm Universe @ NIKA2*, 00012
 de Graaff, A. et al. 2019, *A&A*, 624, A48
 Dicker, S. R. et al. 2014, in *SPIE*, ed. W. S. Holland & J. Zmuidzinas, Vol. 9153, 91530J
 Fukugita, M. et al. 1998, *ApJ*, 503, 518
 Govoni, F. et al. 2009, in *Revista Mexicana de Astronomia y Astrofisica Conference Series*, Vol. 36, CD308–CD311
 Hilton, M. et al. 2021, *ApJS*, 253, 3
 Hincks, A. et al. 2021, *MNRAS*
 Honda, S. et al. 2023, *URSI Radio Science Letters*, 4, 53
 Isopi, G. et al. 2023, *JLTD*, in prep
 Mroczkowski, T. et al. 2019, *Space Science Reviews*, 215
 Murgia, M. et al. 2010, *A&A*, 509, A86
 Orłowski-Scherer, J. et al. 2022, *A&A*, 667, L6
 Paiella, A. et al. 2022, *JLTP*
 Paiella, A. et al. 2023, *JLTD*, in prep
 Perotto, L. et al. 2020, *A&A*
 Reiprich, T. H. et al. 2021, *A&A*, 647, A2
 Romero, C. 2021, *MUSTANG-2 Mapping Speeds*, Tech. rep., NRAO/GBO
 Singari, B. et al. 2020, *JCAP*, 2020, 028
 Sunyaev, R. A. & Zeldovich, I. B. 1980, *ARA&A*, 18, 537
 Tanimura, H. et al. 2019, *MNRAS*, 483, 223
 Tejos, N. 2016, in *IAU Symposium*, ed. R. van de Weygaert, S. Shandarin, E. Saar, & J. Einasto, Vol. 308, 364–367
 Wilson, G. W. et al. 2020, in *SPIE*, ed. J. Zmuidzinas & J.-R. Gao, Vol. 11453, 1145302